Earth's Future

RESEARCH ARTICLE
10.1029/2025EF007795

The Role of Propellant Type, Re-Entry, and Plume Reactions in the Atmospheric Impacts of Spaceflight

Yvar S. W. Vliex[1], Jurriaan A. van't Hoff[1], and Irene C. Dedoussi[1,2]

[1]Operations & Environment, Faculty of Aerospace Engineering, Delft University of Technology, Delft, The Netherlands, [2]Whittle Laboratory, Department of Engineering, University of Cambridge, Cambridge, UK

Key Points:

- Emissions from 61.9 Gg of fuel by spaceflight in 2022 affected the ozone column (−85.6 mDU) and global radiative forcing (+4.1 mW/m^2)
- Plume-scale chemistry and re-entry emissions respectively account for 14.6% and 87.6% of the ozone depletion from spaceflight emissions
- Per payload mass, solid rocket fuels yield the largest ozone depletion, whereas RP1 has the largest effect on climate

Supporting Information:

Supporting Information may be found in the online version of this article.

Correspondence to:

I. C. Dedoussi,
icd23@cam.ac.uk

Citation:

Vliex, Y. S. W., van't Hoff, J. A., & Dedoussi, I. C. (2026). The role of propellant type, re-entry, and plume reactions in the atmospheric impacts of spaceflight. *Earth's Future*, *14*, e2025EF007795. https://doi.org/10.1029/2025EF007795

Received 21 DEC 2025
Accepted 25 APR 2026

Abstract The space industry is growing rapidly, and over the coming years the number of annual rocket launches is expected to increase further. This increases the sector's emissions and environmental effects, both of which are not yet comprehensively understood. Using open-sourced data we develop a four-dimensional emission inventory for spaceflight activities in 2022, incorporating emissions from re-entry and plume chemistry. We assess their effects on the stratospheric composition and radiative forcing using the GEOS-Chem chemistry transport model. We find that spaceflight emissions lead to a annual global column ozone loss of 85.6 mDU and a net radiative forcing of 4.1 mW/m^2. The majority (87.7%) of ozone depletion is driven by NO_x emissions from re-entry, and we show that the inclusion of plume chemistry reduces global ozone depletion by 17.1% and radiative forcing by 29.1%. Among individual propellant types, solid propellant has the largest impact in terms of ozone depletion, causing a reduction of 48.3 mDU per Gg of payload, while RP1-fueled rockets contribute the most to radiative forcing, at 1.9 mW/m^2 per Gg of payload. Our results highlight the need to consider and accurately model re-entry emissions, engine plume reactions and their interactions.

Plain Language Summary Rocket engines emit pollutants in all layers of the atmosphere, and the burn-up of satellites and discarded rocket bodies leads to emissions at high altitudes. As the space industry is expected to continue to grow rapidly, a good understanding of its environmental effects is needed. We compile the emissions from all space activities in 2022 and simulate their impact on the ozone layer and climate. We find that spaceflight leads to a globally averaged depletion of the ozone layer and contributes to global warming. Nearly 88% of the ozone loss comes from nitrogen oxides released by objects re-entering the atmosphere. We also show that accounting for chemical reactions in the rocket exhaust plume during launch reduces the predicted ozone loss and climate impact. Comparing between fuel types, solid propellant has the largest impact on ozone depletion, while rocket-grade kerosene has the largest climate response relative to payload mass.

1. Introduction

The space industry has grown rapidly in recent decades, with the yearly launch rate having more than tripled since 2005 (Ailor, 2019) and the number of operational spacecraft having more than doubled to reach approximately 2900 (Pardini & Anselmo, 2021). Based on current trends such as the privatization of the space industry, the development of reusable boosters, and the plans for satellite mega-constellations and space tourism, the yearly launch and re-entry rates are expected to increase considerably (Boley & Byers, 2021; Brown et al., 2023; Ross & Jones, 2022), with almost 10,000 spacecraft being planned for low-earth orbits in the upcoming years (Maloney et al., 2025; Muelhaupt et al., 2019; Pardini & Anselmo, 2022).

The effects of spaceflight emissions on the atmosphere and climate have long been considered negligible due to their relatively small quantity (Kokkinakis & Drikakis, 2022; Ross & Toohey, 2019), with earlier estimates finding that annual spaceflight emissions are only 0.01% of the annual emissions from aviation (Ross & Sheaffer, 2014). Spaceflight emissions have different vertical distributions compared to aviation emissions however, spanning all layers of the atmosphere. At higher altitudes the emissions have longer lifetimes, increasing their effects on atmospheric composition and radiative forcing (Ross et al., 2010; Ross & Sheaffer, 2014). The direct insertion of emissions into the ozone layer also affects its chemistry, potentially leading to depletion of the ozone column (Ross et al., 2004, 2009).

Earlier studies estimate that emissions from spaceflight decrease the global stratospheric ozone concentration by 0.01%–0.03% (Jackman et al., 1996; Ross et al., 2009; Ryan et al., 2022), with Ross et al. (2010) finding an ozone depletion of several percent for a hypothetical fleet of 1000 hydrocarbon-fueled rockets. Ryan et al. (2022)

determined that ozone depletion is primarily driven by NO_x (51%) and chlorine (49%) emissions. Additionally, the NO_x and alumina emissions from the re-entry of rocket bodies or satellites may have an important effect on ozone depletion (Ferreira et al., 2024; Revell et al., 2025; Ryan et al., 2022; Shutler et al., 2022). Water vapor emissions can lead to the formation of HO_x radicals that catalytically deplete ozone, although this effect is estimated to be limited (Larson et al., 2017; Ryan et al., 2022). Water vapor emissions also contribute to the formation of polar stratospheric clouds that support heterogeneous reactions that form ozone-depleting chlorine radicals (Kelley et al., 2010; Tritscher et al., 2021). Complete ozone destruction has been observed on a local scale through in situ measurements in rocket plumes (Ross et al., 1997, 2000), but ozone levels returned to normal within an hour (Lohn et al., 1999) and these local effects were found to be negligible on a global scale compared to the effects of dispersed emissions (Danilin, Ko, & Weisenstein, 2001; Ryan et al., 2022).

Estimates for the radiative forcing (RF) due to spaceflight emissions range between 3.9 and 16 mW/m^2 (DeSain & Brady, 2014; Ross & Sheaffer, 2014; Ryan et al., 2022), with black carbon (BC) emissions being the dominant contributor. Ryan et al. (2022) found that the RF per unit mass of stratospheric BC emissions is approximately 500 times larger than for aviation. Ross and Sheaffer (2014) demonstrated that alumina particles could also result in positive RF, which they found to account for 28% of the total radiative forcing from spaceflight. The radiative effect of alumina depends highly on the phase, optical properties and size distribution, all of which are subject to considerable uncertainties in modeling (Danilin, Shia, et al., 2001; Maloney et al., 2025; Ross & Sheaffer, 2014; Schmid et al., 2003). Several studies suggest that the RF from water vapor emissions is negligible compared to other pollutants (DeSain & Brady, 2014; Larson et al., 2017; Ross & Sheaffer, 2014; Ryan et al., 2022).

The effective speciation of spaceflight's emissions is likely to change in the future. Four major types of rocket propellant are currently in use: rocket-grade kerosene, liquid hydrogen, hypergolic propellant, and solid propellant (Brown et al., 2023; Dallas et al., 2020), but this is expected to change. Hypergolic propellants are expected to be phased out because of their toxicity (Dallas et al., 2020; Ross & Sheaffer, 2014), and several liquid-methane-fueled rockets are currently being developed (Ross & Vedda, 2018). A shift in propellant usage can have considerable impacts on the environmental footprint of spaceflight because each propellant type has a unique emission profile (Dallas et al., 2020). Furthermore, in situ plume measurements have shown that differences between the exhaust flow composition and expected rocket exhaust emissions (Ross et al., 1997, 2000). Chemical reactions in the plume can oxidize black carbon, nitrogen and carbon monoxide and convert HCl into Cl or Cl_2 (Danilin, Ko, & Weisenstein, 2001; Dallas et al., 2020) and can substantially alter the composition of the exhaust flow (James et al., 2021; Voigt et al., 2013), but are currently unaccounted for.

In this work we aim to quantify the atmospheric impacts of different aspects of spaceflight, focusing on the effects of re-entry emissions, plume scale chemistry, and individual rocket fuels. We model the emissions from rocket launches and re-entries in 2022, provided open-source, and use a three-dimensional chemistry transport model to assess the impact on the atmosphere and climate. We account for the effects of chemical reactions in the rocket plume and provide a comparative analysis of different propellant types.

2. Methods

To estimate the atmospheric impact of spaceflight, we develop a four-dimensional emission inventory for spaceflight emissions in 2022, considering the emission of CO_2, CO, H_2O, BC, NO_x, HCl, Cl and Cl_2. We first simulate the trajectory and combustion process of each rocket up to 100 km altitude to determine the emitted pollutants at each time step and altitude level, and then correct for reactions in the plume that change the chemical composition of the exhaust flow. The emission inventory is subsequently implemented in the GEOS-Chem model to determine its impact on atmospheric composition and radiative forcing. This process is expanded upon in the subsequent sections.

2.1. Emissions Modeling

We simulate 186 rocket launches and 472 re-entry objects for 2022 (ESA, 2025; Krebs, 2022). Figure 1 shows the geographic distribution of the launches. 95% of all rocket launches occurred in the Northern Hemisphere. For around 6% of the rocket launches, data needed to simulate their trajectory is missing and is instead estimated based on comparable rockets in the same launch vehicle class, based on their low-earth orbit payload capability as defined by NASA (McConnaughey et al., 2012).

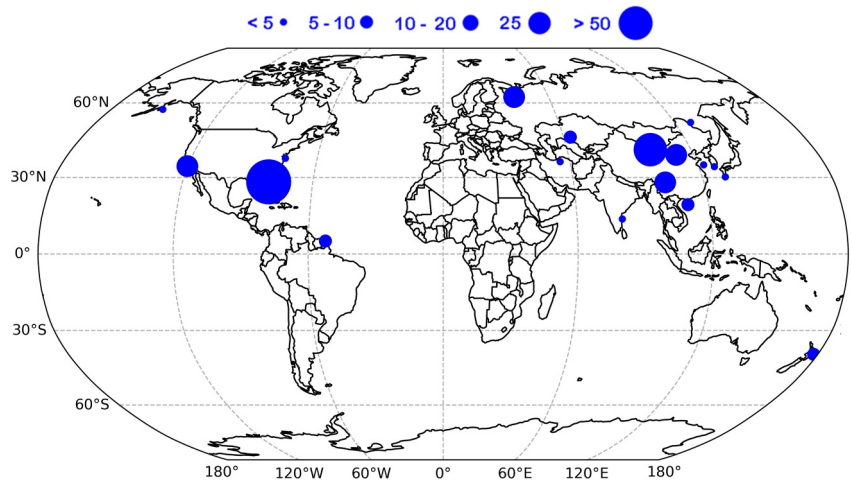

Figure 1. Locations and number of rocket launches in 2022, with marker size indicating launch frequency.

Five propellant types were used in 2022 (Krebs, 2022): RP1 (liquid rocket-grade kerosene and liquid oxygen), LH2 (liquid hydrogen and liquid oxygen), UDMH (liquid unsymmetrical dimethylhydrazine and liquid nitrogen tetroxide), solid (solid aluminum and solid ammonium perchlorate with a hydrocarbon binder) and LCH4 (liquid methane and liquid oxygen) (Dallas et al., 2020). We do not include the liquid methane rocket launch in our inventory because there are no measurements or estimates of its emission profile. As it is only a single rocket launch, we expect its exclusion to have little effect on the total inventory.

The trajectory of the rockets is modeled as a vertical launch followed by a gravity turn, where the rocket is treated as a point mass. The model consists of a set of ordinary differential equations based on standard rocket motion, comparable to the approach from Pradon et al. (2023). The altitude, speed, flight path angle and horizontal distance are computed by solving these differential equations using the Runge-Kutta-Fehlberg method (Fehlberg, 1970). Thrust and mass flow are modeled as a function of time and are based on the characteristics of each engine. Drag is calculated using the drag equation, where the drag coefficient C_D is modeled as a function of Mach number (Casalino et al., 2022) and is considered the same for each rocket. More details on the modeling of trajectories can be found in Text S1 of Supporting Information S1. Throttling of liquid rocket engines is excluded due to a lack of available throttling profiles. As the target orbit and payload data is not publicly available for all missions, we simulate a nominal trajectory for each rocket based on the low Earth orbit payload capacity. This approach may underestimate propellant usage for missions requiring higher energy orbits or carrying heavier payloads, consequently underestimating their total atmospheric impact. We find a 7% difference in simulated propellant expelled for a Falcon 9 trajectory compared to the reference telemetry shown in Text S1 of Supporting Information S1.

We include thermal NO_x emissions produced by the re-entry and burn-up of space debris and the controlled re-entry of rocket stages. We do not include emissions produced by the burning of propellant during re-entry, as the Falcon 9 only reserves 6% of total fuel mass for controlled re-entry and landing (Kim et al., 2021). We use DISCOS (Database and Information System Characterizing Objects in Space) from the European Space Agency (Torre et al., 2001) to track and geolocate space debris from payloads and rocket stages outside of the atmosphere. We find a total mass influx from re-entry of 4899 tons, of which 14% comes from payloads and satellite bodies and 86% comes from rocket stages. This is similar to the 4929 tons of re-entry mass in 2022 found by Barker et al. (2024).

We estimate the thermal NO_x emissions to be 17.5% of the re-entry mass for reusable components (Larson et al., 2017; Park & Rakich, 1980) and 100% of the re-entry mass for discarded objects (Ryan et al., 2022). This simplification introduces uncertainty, but a more accurate estimation would require the re-entry velocity, trajectory and surface area of each object (Park, Navarro Laboulais, Leyland, & Mischler, 2021), which are not available. We model the vertical distribution of NO_x for the burn-up of rocket stages following the trajectory defined by Park, Navarro Laboulais et al. (2021). For the re-entry of satellite objects, we adjust the trajectory to

Table 1
Equations for the Final Emission Index of Different Species Following the Plume Reactions

Species	Equation	Source
H_2O	$EI_f(H_2O) = EI_e(H_2O) + \frac{MW(H_2O)}{MW(H)}EI_e(H) + \frac{MW(H_2O)}{MW(H_2)}EI_e(H_2) + EI_e(OH)$	As reported in James et al. (2021)
CO_2	$EI_f(CO_2) = EI_e(CO_2) + \frac{MW(CO_2)}{MW(CO)}\left[EI_e(CO) - EI_f(CO)\right]$	Derived from James et al. (2021)
NO_x	$EI_f(NO_x) = EI_e(NO_x) + 39.456e^{-0.130h} - 1.659$	Based on data from Leone and Turns (1994)
HCl	$EI_f(HCl) = EI_e(HCl) + EI_p(HCl)$	Based on data from Leone and Turns (1994)
Cl	$EI_f(Cl) = EI_e(Cl) + EI_p(Cl)$	Based on data from Leone and Turns (1994)
Cl_2	$EI_f(Cl_2) = EI_e(Cl_2) + EI_p(Cl_2)$	Based on data from Leone and Turns (1994)
BC	$EI_f(BC) = 0.030 \cdot \max\left\{0.04, \min\left[0.5, 0.04e^{0.12(h-15)}\right]\right\}$	Derived from James et al. (2021)

Note. The subscripts *e*, *p*, and *f* denote the emission index at the engine exhaust, in the plume and the effective emission index, respectively, and *h* is the altitude in kilometers.

ensure the peak ablation altitude occurs at 78 km, consistent with the altitude profile from the ATmospheric Impact of SPAcecraft Demise project by the European Space Industry (Bekkki et al., 2021) and the work by Maloney et al. (2025). We do not consider other emission species that are formed through ablation such as Al_2O_3, $MgAl_2O_4$, ZnO and TiO_2 as they are only emitted in limited quantities and are not included in the GEOS-Chem model.

Because the horizontal travel distance of rockets is less than half the size of our model grid cells, rocket launch emissions are included as vertical columns over the launch site, similar to the findings by Pradon et al. (2023). Rocket stages that are discarded below 100 km and their thermal NO_x emissions are modeled at the same latitude and longitude as the original launch. Emissions from objects re-entering the atmosphere are confined to the grid cell corresponding to the reported re-entry location.

We use the Chemical Equilibrium with Applications (CEA) model (McBride & Gordon, 1994) to determine the primary emissions (defined as the pollutant mass per mass of propellant burned at the rocket nozzle exit) based on the mixing ratio between the fuel and oxidizer, the chamber pressure, and the area ratio between the nozzle and the throat. The theoretical rocket performance is modeled by the one-dimensional conservation equations for mass, momentum and energy, and we assume isentropic expansion in the nozzle and complete adiabatic combustion in the combustion chamber. The flow is modeled with reactions occurring until the throat of the nozzle, as this was deemed to most accurately represent reality (Garner, 2022). CEA can only model complete combustion, meaning that black carbon is not included, and does not account for the formation of thermal NO_x. Consequently, these two species are modeled separately as discussed in the next section.

2.2. Plume Reactions

Reactions in the exhaust plume can affect BC, CO, CO_2, H_2O, NO_x and chlorine species, and these can vary with altitude (Danilin, Ko, & Weisenstein, 2001). We therefore define secondary emissions as those formed in the plume and final effective emissions as those dispersed into the atmosphere. We estimate these using measurements and simulations from past works (Gomberg & Stewart, 1976; James et al., 2021; Leone & Turns, 1994; Malkin, 1978; Zittel, 1994). Table 1 shows the equations for the final effective emission index of different species. Based on earlier measurements (Gomberg & Stewart, 1976; Malkin, 1978), we assume that all hydrogen and hydroxyl in the plume is converted into H_2O. To determine the final emission index of CO, we use a least-squares regression using numerical simulation data of plumes of the Space Shuttle and Titan IV (Denison et al., 1994; Gomberg & Stewart, 1976). Similar regressions are set up for HCl, Cl and Cl_2 by combining data of multiple studies (Gomberg & Stewart, 1976; Leone & Turns, 1994; Zittel, 1994). The thermal NO_x model is obtained by fitting an exponential curve to the data from Leone and Turns (Leone & Turns, 1994) on the formation of thermal NO_x in the plume of the Space Shuttle. More details on these models are provided in Text S2 of Supporting Information S1.

2.3. Atmospheric Modeling

To simulate the impact of spaceflight emissions, we use the GEOS-Chem atmospheric chemistry-transport model. Specifically, we use the GEOS-Chem High-Performance model version 14.3.0 with the Unified Tropospheric-Stratospheric Chemistry Extension (UCX) (Eastham et al., 2014), coupled with the Rapid Radiative Transfer Model for General Circulation Models (RRMTG) (Heald et al., 2014). The model is driven by the Modern-Era Retrospective analysis for Research and Applications version 2 (MERRA-2) meteorology (Gelaro et al., 2017). Photolysis rates are calculated using the Cloud-J calculation code (van Caspel et al., 2023). The non-CO_2 radiative forcing is calculated at the Top-of-Atmosphere (TOA) and includes the stratospheric adjustments as implemented by Eastham et al. (2022).

The model is spun-up for 7 years without space sector emissions, after which the spaceflight emissions are injected and the simulations are performed for 2 years. The simulations are run using a cubed-sphere grid with a resolution of C24 (roughly 400 by 500 km) and 72 vertical pressure levels up to an altitude of 80 km. Similar model resolutions have been used in past studies of high-altitude emissions (van't Hoff et al., 2024; Ryan et al., 2022; Eastham et al., 2022). This resolution was chosen for its lower computational time and cost, given that we evaluate multiple emission scenarios. It has been reported that similar horizontal resolutions led to excessive horizontal mixing and enhanced stratosphere-troposphere exchange compared to higher horizontal resolutions (Stanevich et al., 2020; Strahan & Polansky, 2006), but Eastham et al. (2022) found the mean age-of-air to be within 6 months of reference data with a similar horizontal resolution in the GEOS-Chem model.

We use fixed surface mixing ratios for methane and other long-lived species, as prescribed by historical data from NOAA (Murray, 2016). This means our model may not capture long-term methane feedback loops, which Eastham et al. (2022) have shown can increase the total ozone depletion by up to 15% in response to supersonic aircraft emissions. Because our model integration time is shorter than their 42 years interval, we expect that any underestimation from the lack of methane feedbacks may however be smaller.

2.4. Emission Scenarios

We simulate seven different spaceflight emission scenarios along with a baseline scenario (no spaceflight emissions). We consider a nominal scenario with spaceflight emissions from 2022, including re-entry of space debris and rocket stages and plume-scale reactions. To isolate the effect of individual propellants, re-entry and plume reactions, we evaluate scenarios where emissions from these individual sources are excluded. When excluding a specific propellant type, we exclude emissions from all stages that use that propellant, emissions from other stages with different propellants are kept. For example, in the emissions scenario without solid propellant we exclude emissions from the Ariane V's solid boosters, but keep the emissions of the core stages. To better compare the effects of individual propellants, we normalize the ozone depletion and radiative forcing per Gg of propellant burned and per Gg of payload to Low Earth Orbit (LEO) capacity. In this calculation we assume the maximum reported LEO payload capacity for each rocket.

3. Results and Discussion

The spaceflight emissions for 2022 are presented in Section 3.1, together with the effects of plume reactions and re-entry on the emitted quantities. Their impact is then quantified in terms of atmospheric composition (Section 3.2) and radiative forcing (Section 3.3) for all emission scenarios. Lastly, the limitations of this study are discussed in Section 3.4.

3.1. Spaceflight Emission Inventory

Table 2 shows all the emission inventories for the scenarios described in Section 2.1. The total propellant burned in the nominal scenario is 61.9 Gg, the majority of which is RP1 (43.6 Gg), followed by UDMH (9.6 Gg), solid fuels (5.5 Gg), and LH2 (3.2 Gg). In comparison, the 2022 spaceflight fuel burn is approximately 0.021% of the annual fuel burn from civil aviation in 2019 (Quadros et al., 2022). In this scenario, the CO_2, H_2O and NO_x emissions are respectively 0.0042%, 0.0058% and 0.078% of the aviation attributable emissions for 2019 (Quadros et al., 2022).

Figure 2 shows the distribution of emissions per propellant type and launch site. 99% of the total emissions occur in the Northern Hemisphere. The majority of the emissions are from launches originating in the United States,

Table 2
Annual Emissions and Annual Averaged Atmospheric and Radiative Impacts for Different Spaceflight Scenarios

	Nominal	RP1	LH2	UDMH	Solid	Re-entry	Plume effects
Emissions							
Fuelburn [Gg]	61.9	43.6	3.2	9.6	5.5	–	–
CO [Gg]	0.5	0.4	0	0.049	0.0	0	−0.9
CO_2 [Gg]	37.0	30.9	0	4.0	2.1	0	0.4
H_2O [Gg]	20.3	13.3	1.9	3.4	1.7	0	0
BC [Gg]	0.4	0.4	0	0.0	0.0	0	−0.8
NO_x [Gg]	3.5	0.4	0.0	0.1	0.1	2.9	−0.3
HCl [Gg]	0.7	0	0	0	0.7	0	−0.7
Cl_x [Gg]	0.3	0	0	0	0.3	0	0.3
Impacts							
O_3 [mDU]	−85.6	5.4	−0.3	0.4	−14.7	−75.0	12.5
H_2O [Gg]	140.2	69.8	3.6	15.8	22.1	29.1	−19.2
NO_x [Gg]	11.9	−0.2	−0.0	0.0	−0.1	12.2	−0.6
BC RF [mW/m^2]	8.2	6.9	0.0	0.9	0.3	0.2	−3.6
H_2O RF [mW/m^2]	−1.4	−1.3	−0.1	−0.3	−0.1	−0.1	0.8
O_3 RF [mW/m^2]	−2.6	−2.2	0.1	−0.4	−0.4	−0.2	1.1
CH_4 RF [mW/m^2]	−0.1	−0.1	−0.0	−0.0	−0.0	−0.0	0.0
Total RF [mW/m^2]	4.1	3.4	0.1	0.3	−0.2	−0.0	−1.7

Note. The re-entry scenario includes thermal NO_x emissions that result from the re-entry and burn-up of space debris and controlled re-entry of rocket stages. Plume effects refer to the chemical reactions in the rocket exhaust plume during launch. All scenarios are calculated in reference to the baseline emissions, except the plume effects which is in reference to the nominal scenario. Changes in chemical species are presented as the change in global column ozone [mDU] and in the stratospheric mass (H_2O, NO_x and BC). Radiative forcing is calculated at the Top-of-Atmosphere.

accounting for 64.3% of the total emissions from 41.9% of the launches. This is followed by launches from China, accounting for 21.8% of emissions and 32.8% of launches. The relatively lower emissions per launch in China are related to the higher proportion of small-lift launch vehicles compared to the United States. A higher proportion of solid rockets were launched in India and French Guiana, therefore these regions have higher proportions of HCl, Cl, and Cl_2 emissions.

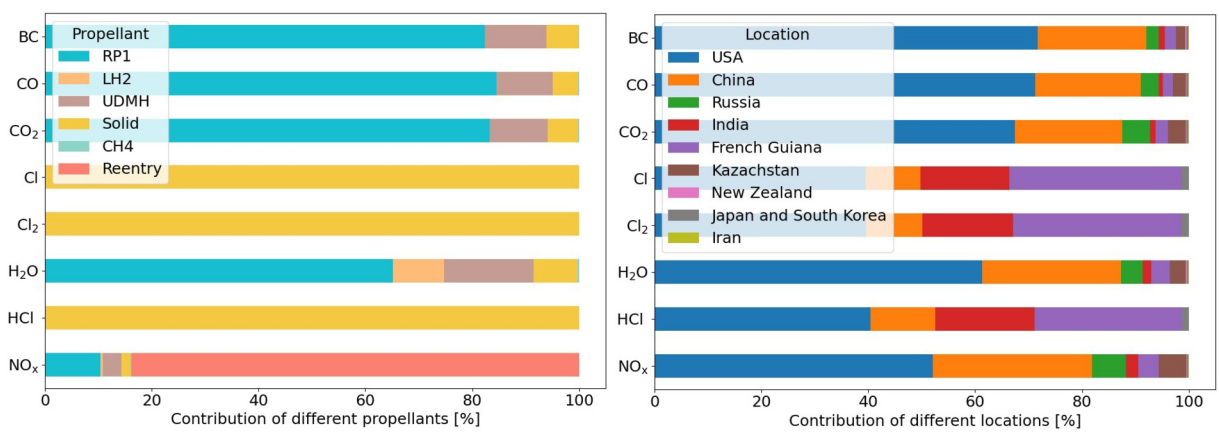

Figure 2. Spaceflight emissions mass contributions for 2022 per propellant type (left) and launch location (right).

10.1029/2025EF007795

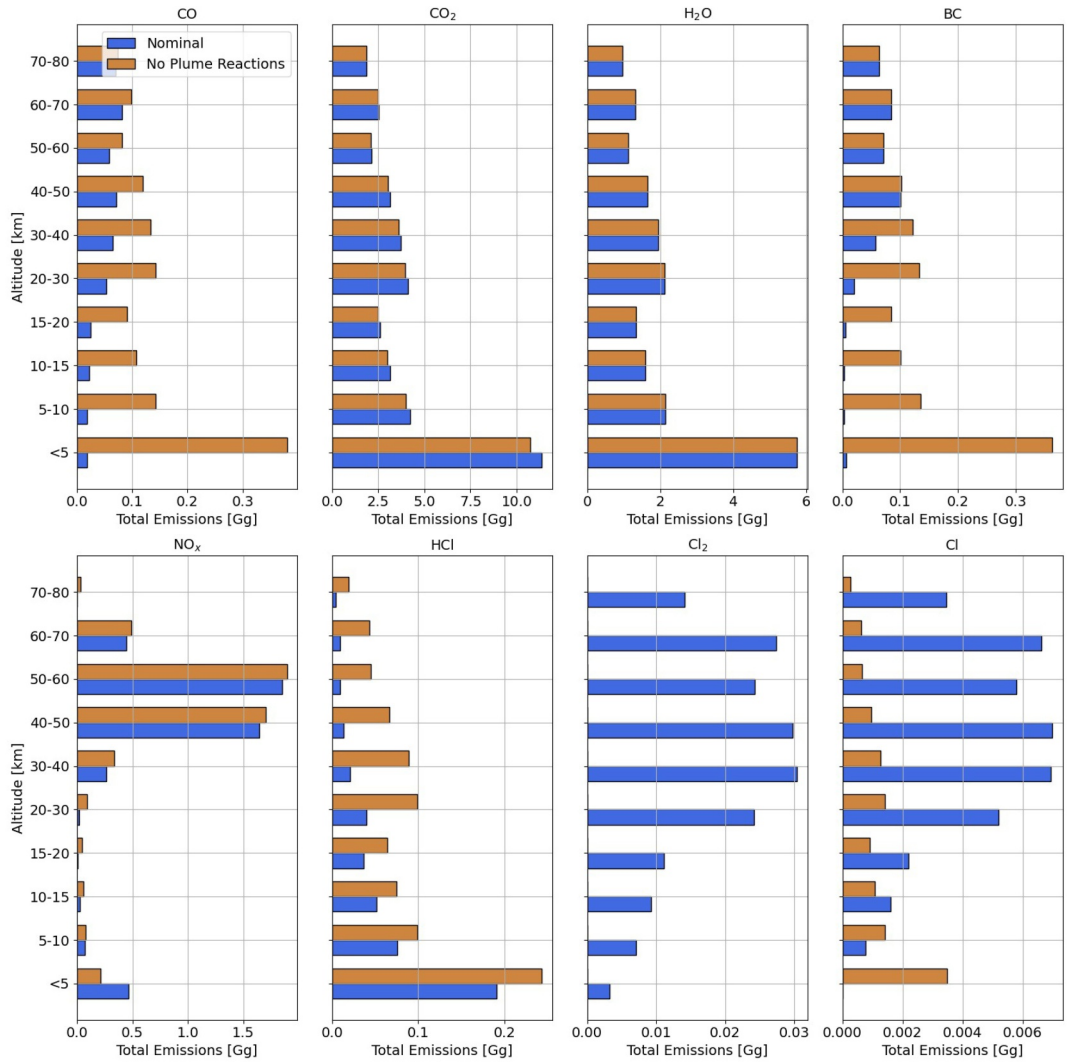

Figure 3. Vertical distribution of the total spaceflight emissions in 2022 [Gg] for the nominal scenario and the scenario without plume effects. Cl_2 emissions are not modeled separately in the scenario without plume effects, instead, it is all assumed to be emitted as Cl.

RP1-fueled rockets produce 60%–80% of the total CO, CO_2, H_2O and BC emissions, which is to be expected since they account for the majority of the launches (60%) and propellant mass burned (70.5%) and have the highest carbon fraction of all propellant types. Liquid hydrogen rockets produce 9.5% of all H_2O emissions at only 3.4% of the total launches, a result of the emission index of H_2O being close to 1.00 and the large size of the liquid hydrogen rockets that were launched such as the Delta IV-Heavy and the Space Launch System. Re-entry accounts for 83.9% of the total NO_x emissions, which is comparable to the results from Ryan et al. (2022) and Revell et al. (2025).

We find that including plume reactions reduces BC emissions by 66.8% and NO_x emissions by 7.1%. The reduction in BC emissions is related to increased oxidation of BC to CO or CO_2 in the plume, and NO_x emissions are reduced as the reaction of N_2 and O_2 decreases with altitude. Figure 3 highlights the strong altitude dependencies on the chemical reactions in the rocket plume. In the nominal scenario, the amount of BC emissions in the troposphere and lower stratosphere (below 30 km) is reduced by 95.4% compared to the scenario without plume reactions. NO_x emissions from launch vehicles are reduced by 35.8% above 15 km. While HCl emissions decline when including plume effects, emissions of Cl and Cl_2 increase.

Table 3
Comparison of Fleet-Averaged Emission Indices [g/kg] With Past Literature for the Nominal Emission Scenario

	CO_2	H_2O	BC	NO_x	Cl_y
This Work					
RP1	853	304	8.8	10.4	0
LH2	0	1003	0	4.5	0
UDMH	506	431	6.0	14.5	0
Solid	360	290	4.0	11.1	152.4
Ryan et al. (2022)					
RP1	–	300	35	14	0
LH2	–	1000	0	33	0
UDMH	–	550	4	20	0
Solid	–	370	4	3	213
Ross and Sheaffer (2014)					
RP1	600	350	10–40	–	0
LH2	0	1000	0	–	0
UDMH	150	550	2–8	–	0
Solid	200	350	2–8	–	–
Barker et al. (2024)					
RP1	637	340	22	0	0
LH2	0	1058	0	0	0
UDMH	150	392	16	10	0
Solid	112	302	16	0	217
Brown et al. (2024)					
RP1	600	350	20	0	0
LH2	0	1000	0	33	0
UDMH	200	550	20	20	0
Solid	300	370	20	3	210

Compared to the 2022 spaceflight emissions inventory of Barker et al. (2024), we find very similar levels of fuel burn (61.9 Gg compared to 63 Gg) and similar levels of global emissions. Barker et al. (2024) report roughly 190% higher CO and roughly 15% CO_2 emissions compared to our inventory, whereas we find around 75% higher NO_x emissions. The former is a result of us using a lower emission index for CO, while the latter is primarily from re-entry, as we assume higher fractions of NO_x emissions for re-entry mass (100%) than Barker et al. (2024) (40%). Compared to the emission inventory from Ryan et al. (2022) for 2019 (which had 103 launches and different types of rocket launched), we find 89.5% more H_2O, 57% more NO_x and 18% less BC emissions. This is partially because of differences in fuel usage. In 2019 29% of the rocket launches used solid propellant, but this is reduced to 10.5% in 2022 which has a higher share RP1-fueled rockets, leading to an increase in RP1 fuel burn of 33% compared to 2019. To facilitate comparison with other works we calculate the fleet-averaged emission indices per propellant type, which are presented in Table 3. As a result of including plume reactions, we find a 75% lower BC emission index for RP1 compared to Ryan et al. (2022), which is close to the lowest estimate made by Ross and Sheaffer (2014). We also find a 88% higher NO_x emission index for LH2 and a 270% higher emission index for solid propellant as a result of modeling plume NO_x plume reactions.

3.2. Atmospheric Composition Changes

Table 2 summarizes the global mean change in column ozone, stratospheric H_2O and NO_x mass and radiative forcing for all scenarios. We find that the 2022 spaceflight emissions reduce the global ozone column by 85.6 mDU for the nominal scenario. This is roughly 2.5 times the value found by Ryan et al. (2022) for 2019. This is likely caused by the fact that we find 47% more NO_x emissions than Ryan et al. (2022), of which 73% occur between 40 and 60 km while they find 95% of the total NO_x emissions above 60 km. This may also be affected by our use of a 72 vertical layer model grid, instead of the 47 layers used by Ryan et al. (2022). We also find 5.5% more Cl_x emissions (defined as HCl + Cl + Cl_2), but we do not include Cl activation due to alumina particles. The ozone column loss we find is smaller than that reported by Ross et al. (2009) for 2009 spaceflight emissions (102 mDU), who calculate the global ozone loss with a parameterized approach instead of using a chemical transport model.

Figure 4 shows the spatial distribution of the atmospheric change for O_3, H_2O, NO_x and BC. It shows that spaceflight emissions lead to loss of stratospheric ozone in the northern hemisphere, and the accumulation of H_2O, NO_x, and BC. We find that this leads to net depletion of the ozone column in the mid-latitudes and polar regions of the Northern Hemisphere, with a peak column ozone decrease of 200.0 mDU in the Arctic region. These ozone losses are offset by a weaker increase of ozone in the lower stratosphere. Similar ozone responses have also been reported in studies of the effects of emissions from supersonic aircraft (Eastham et al., 2022; Zhang et al., 2023; van't Hoff et al., 2024, 2025). The lower-stratospheric net-increase in ozone may be the result of the self-healing properties of ozone (Zhang et al., 2021a) where ozone destruction at high altitudes increases the ozone production at lower altitudes by absorbing UV-radiation (Solomon et al., 1992), and the ozone production from NO_x (Grenfell et al., 2006; Larson et al., 2017). We note that we do not explicitly account for changes in aerosol surface area associated with BC, which would lead to additional lower stratospheric ozone loss resulting from enhanced heterogeneous reactions on BC aerosols (Maloney et al., 2022), thus indicating that our modeled increase in lower-stratospheric ozone may be overestimated. Despite the changes in stratospheric ozone and BC, their corresponding surface-level changes (which can be seen as a measure of air quality) are almost negligible. More information on the surface-level changes can be found in Text S3 of Supporting Information S1.

The scenario without plume effects leads to a column ozone decrease of 98.1 mDU. As shown in Figure 3, plume reactions considerably alter the profile and quantity of HCl and Cl_x emissions. We furthermore find a 16.5%, 3.6%

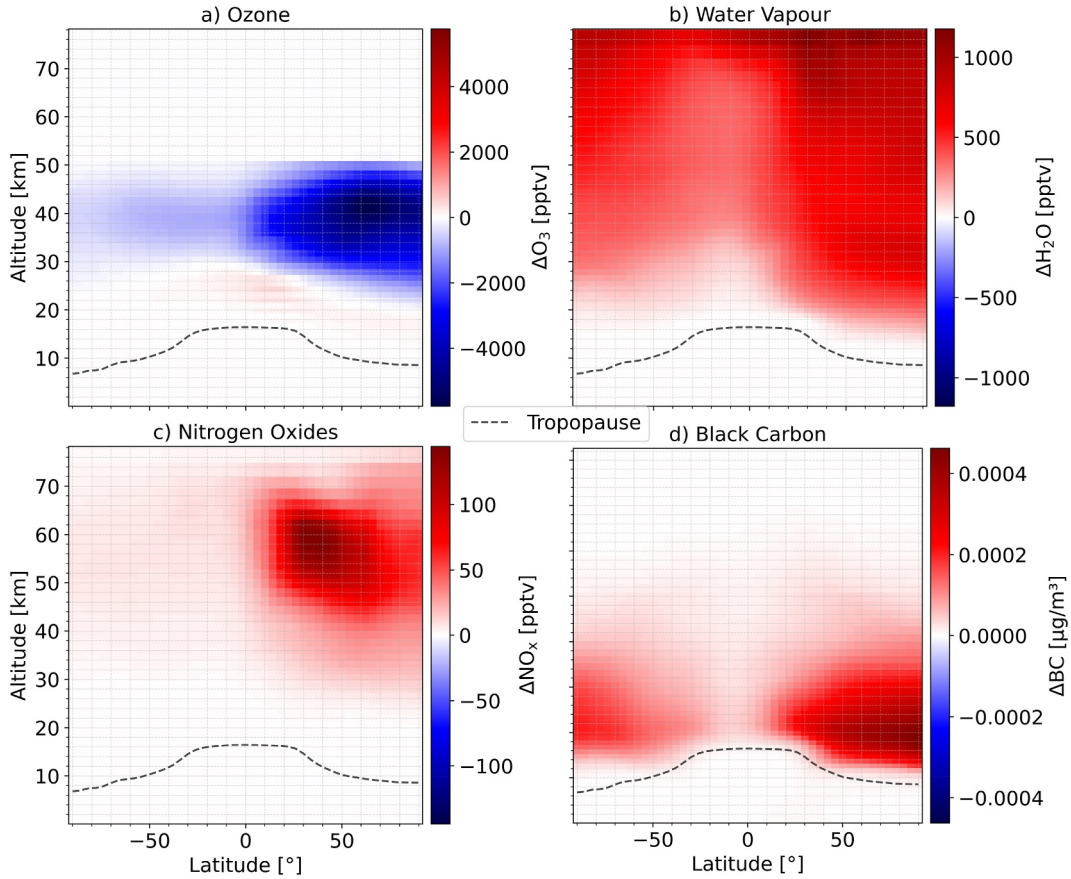

Figure 4. Annual average atmospheric concentration changes of O_3, H_2O, NO_x [pptv] and atmospheric mass concentration changes of BC $[\mu g/m^2]$ due to 2022 spaceflight emissions.

and 45.5% increase in stratospheric H_2O, NO_x and BC mass compared to the nominal scenario. Although plume reactions alter the vertical emission profile of BC, HCl and NO_x, the vertical distribution of the mass burden increase shows a similar vertical pattern to the scenario where it is excluded. This likely indicates that the exact altitude of emissions is less important to the mass burden change than the overall emitted quantity. Nevertheless, our results contradict past assumptions that plume reactions only affect the troposphere (Bennett et al., 1992; Ross & Sheaffer, 2014; Ryan et al., 2022), and show that it should be included in future assessments of rocket emissions. We also find that re-entry emissions account for 87.7% of the total global column depletion because of the large stratospheric NO_x burden increase.

To determine the contributions of individual species to the ozone decrease, we investigate the global annual average odd oxygen (defined as $O_x = O + O_3$) loss rates. Similar to Zhang et al. (2021b), we consider the Chapman cycle (O_x - O_x loss), and the NO_x, HO_x and combined ClO_x and BrO_x loss cycles. Figure 5 provides the odd oxygen loss for the standard spaceflight scenario (a), and the scenarios without plume reactions (b) and re-entry emissions (c). It shows that O_x loss rates from NO_x increase between altitudes of 30 and 50 km in response to the nominal emissions. At the same time the reduction of O_x availability results in reductions of upper-stratospheric O_x loss from the Chapman cycle and HO_x. The spaceflight emissions have the smallest effect on O_x loss from BrO_xClO_x. We note that the model we use does not capture dynamical feedbacks such as temperature changes, which would further affect O_x loss rates (Salawitch et al., 2019; van't Hoff et al., 2025).

Plume reactions have the largest effect on the ClO_x/BrO_x cycle while having a limited effect on the magnitude of other cycles. As shown in Figure 5c, the NO_x cycle is driven by the re-entry emissions. Without re-entry emissions, losses from the BrO_x and ClO_x are dominant and stronger than in the nominal scenario. This is likely because the majority of NO_x emissions are removed without re-entry, reducing the conversion of chlorine and bromine into reservoir species and increasing the availability of O_x by removing NO_x-driven losses (Zhang

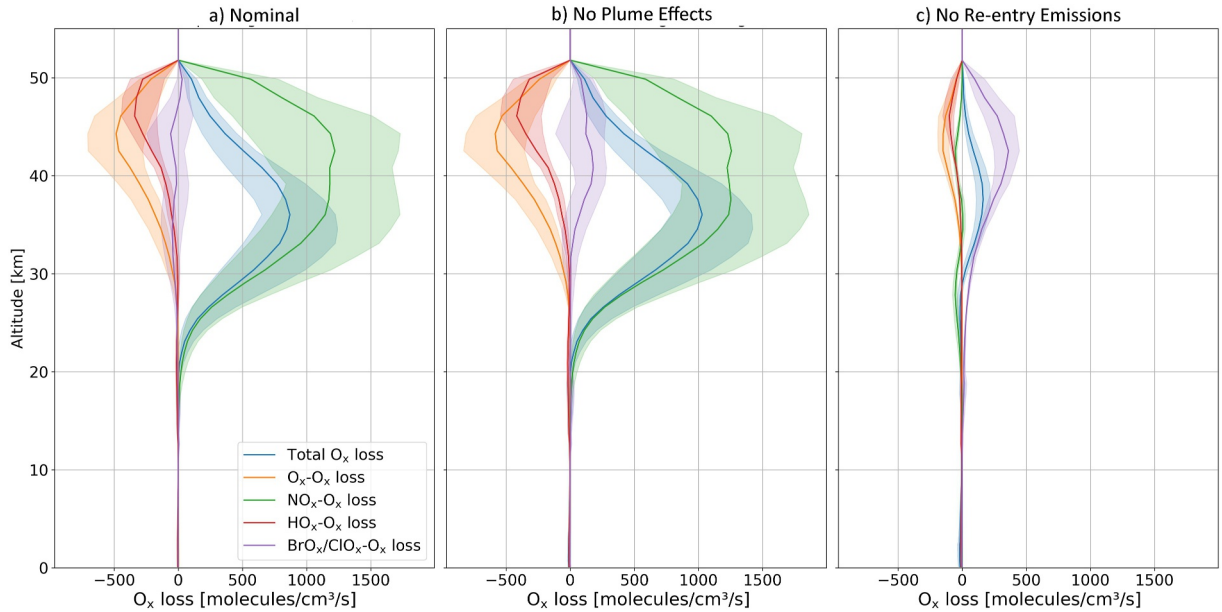

Figure 5. Global annual average oxygen chemical loss rates due to different loss cycles for the 2022 spaceflight emissions (a), the 2022 emissions without plume effects (b) and the 2022 emissions without re-entry emissions (c). The shaded regions show the monthly variation throughout the year.

et al., 2021b). The reduced dominance of NO_x-driven losses subsequently also affects all other cycles due to the increased availability of O_x. Similar effects on O_x loss rates were reported by Zhang et al. (2021a) and van't Hoff et al. (2025) for supersonic aviation emissions. Compared to estimates of spaceflight by Ryan et al. (2022), we find a smaller relative contribution to ozone depletion from ClO_x compared to the 50% from Ryan et al. (2022). This is likely because we find higher NO_x emissions which sharply reduce the effect of chlorine, and we do not capture the impact of alumina particles on the formation of chlorine.

Figure 6a shows the global column ozone change per Gg of propellant burned. We find that solid-fueled rockets have the largest ozone depletion per unit propellant mass of all propellant types (−2.7 mDU/Ggyr), due to their HCl and Cl_x emissions. The effect of solid propellant is likely underestimated as we do not account for heterogeneous reactions on alumina particles emitted by solid rocket engines. Jackman et al. (1998) reported that this inclusion increased ozone depletion by 78.6%, although Danilin, Shia, et al. (2001) later revised this to a 7% increase when accounting for the effects of the particle size distribution of alumina. Ryan et al. (2022) found that Al_2O_3 accounted for 0.3% of the total ozone depletion from spaceflight.

We find that LH2-fueled rockets lead to relatively small ozone depletion compared to the other fuels (−0.1 mDU). While water vapour emissions can deplete ozone by producing hydroxyl radicals, the primary impact stems from an increased loss via the BrO_x/ClO_x cycle. For RP1 and UDMH, we find a net column ozone increase of 0.12 mDU and 0.04 mDU respectively. We find similar results in terms of the column ozone depletion per Gg of payload to LEO capacity (Figure 6c).

3.3. Radiative Forcing

Table 2 shows the Top-of-Atmosphere radiative forcing from different species for all scenarios considered. We estimate radiative forcing from CO_2 using the same method as Zhang et al. (2023). We calculate the increase in atmospheric CO_2 mixing ratio from spaceflight emissions, assuming that the emitted CO_2 is well-mixed, and an atmospheric mass of $5.148{\cdot}10^{18}$ kg (Trenberth & Smith, 2005). Using 16.78 mW/m^2 per ppmv CO_2 increase (Intergovernmental Panel on Climate Change (IPCC), 2001), the 2022 CO_2 emissions from spaceflight lead to an estimated RF of $8.0{\cdot}10^{-6}$ mW/m^2. This is 5 orders of magnitude smaller than the non-CO_2 RF from spaceflight, which agrees with results from Ross and Sheaffer (2014). Because the effect from CO_2 is negligible, we focus on the non-CO_2 effects in the rest of this section.

10.1029/2025EF007795

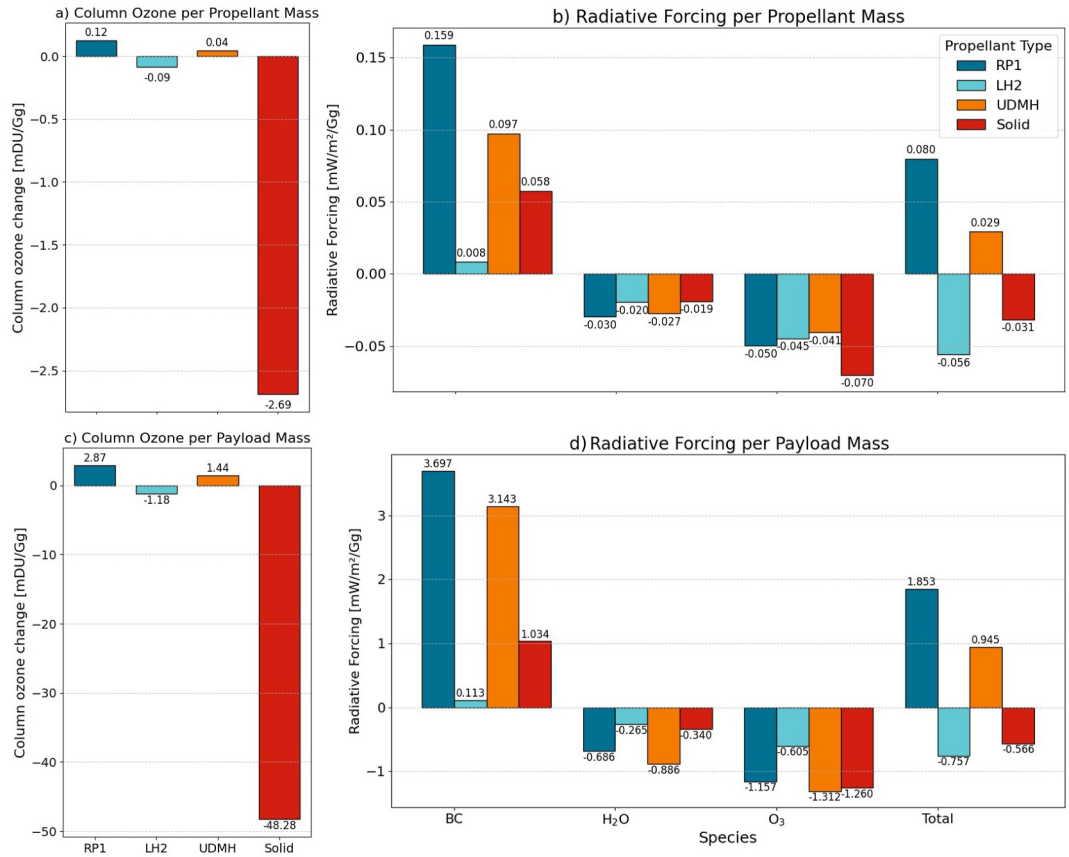

Figure 6. Column ozone depletion and radiative forcing of individual propellant per Gg of yearly propellant burned and per Gg of payload to LEO capacity.

In the nominal emission scenario, we find a net non-CO_2 RF of 4.1 mW/m^2 for a total of 61.9 Gg of propellant burned. This ratio is much higher than for aviation—for example, Lee et al. (2021) found a non-CO_2 RF of 114.8 mW/m^2 for 327 Tg of fuelburn in 2018. RF from spaceflight is driven by warming from BC accumulation (8.2 mW/m^2), and cooling from changes in ozone (−2.6 mW/m^2) and water vapor (−1.4 mW/m^2). The net RF is comparable to the values found by Ryan et al. (2022) (3.9 mW/m^2), but we find a 1.9 times higher radiative forcing for BC even though we have 18% less annual BC emissions. From their results we calculate they have a BC perturbation lifetime of 22 months, whereas we find a perturbation lifetime of around 48 months in our result. This could be driven by differences in the modeling of processes like aerosol deposition, but we also use a finer vertical model grid of 72 layers compared to their 47 layers. The density of the vertical model grid affects the modeling of circulation patterns (Chávez et al., 2022) and this has also been implied to affect stratospheric emission lifetimes (van't Hoff et al., 2025). Our BC lifetime result does agree well with the results of Maloney et al. (2022). Ross and Sheaffer (2014) find a RF of 11 mW/m^2 (1.4×) for 1.5 Gg of BC emissions (3.7×), but they do not make use of a chemistry transport model. We find a larger BC RF per Gg of emissions than previous studies, likely attributed to having a higher proportion of the BC emissions above 20 km. At higher altitudes, BC has a longer lifetime and larger climate impact (Ban-Weiss et al., 2012; Kravitz et al., 2012; Ross & Sheaffer, 2014; Ryan et al., 2022). For instance, Hodnebrog et al. (2014) found that a 40% lifetime reduction can reduce the RF by a factor 2. Excluding reactions in the rocket plume increases the net BC RF by a factor of 1.44 despite tripling the total BC emissions, because the majority of these additional emissions occur in the troposphere. At the timescale we assess, we find that the RF from changes in stratospheric methane is limited.

We find a net RF from H_2O of −1.4 mW/m^2. Our H_2O RF is larger than the −0.20 mW/m^2 found by Ryan et al. (2022) for 2019 spaceflight emissions. This may be because we consider the stratospheric adjusted radiative forcing. It is also likely influenced by our higher vertical model resolution, which has been linked to higher water

vapor perturbation lifetimes (van't Hoff et al., 2025), contributing to more radiative forcing. Ryan et al. (2022) attribute the negative RF to the enhanced formation of polar stratospheric clouds. Several studies have found a net cooling effect from polar stratospheric clouds (Blanchet, 1985; Hicke & Tuck, 2001; Pollack & McKay, 1985). We find the largest negative radiative forcing during the Antarctic winter, coinciding with the peak increase in polar stratospheric cloud surface area.

Our radiative forcing from ozone (-2.6 mW/m^2 in the nominal scenario) is higher than the -0.016 mW/m^2 found by Ryan et al. (2022). Stratospheric ozone decrease leads to a negative radiative forcing (Checa-Garcia et al., 2018; Ramaswamy et al., 2018), and our ozone depletion, which is 2.5 times larger, likely accounts for parts of this disparity, especially since some studies have shown that the radiative forcing from ozone does not scale linearly with total column ozone (Chiodo & Polvani, 2022; Lacis et al., 1990). It may also be affected by our use of stratospherically-adjusted RF. Re-entry emissions account for 87.7% of the total ozone depletion, yet only cause a radiative forcing from ozone of -0.2 mW/m^2. Comparatively, RP1-fueled rocket cause an ozone increase of 5.4 mDU and an ozone RF of -2.2 mW/m^2.

As shown in Figure 6b, we find that RP1-fueled rockets cause the largest positive RF per unit of propellant mass (0.1 mW/m^2/Gg), followed by UDMH-fueled rockets (29 μW/m^2/Gg). We find a net negative RF for LH2 and solid-fueled rockets (-0.1 mW/m^2/Gg and -31 μW/m^2/Gg), a result of the negative radiative forcing from H_2O and O_3 and the reduced BC emissions for these fuels. As shown in Figure 3, RP1 has the largest BC emission index of all species and the proportion of BC emitted in the stratosphere is higher for RP1-fueled rockets (59% compared to 48% and 47% for UDMH and solid, respectively). We find a negative radiative forcing from H_2O and O_3 for all propellant types, even though we find a small column ozone increase for RP1 and UDMH, and a decrease for LH2 and solid propellant. We find comparable results when looking at the RF per payload mass to LEO (Figure 6d),although UDMH-fueled rockets account for a larger fraction of the positive RF (38% and 27%, respectively).

Our results differ from the instantaneous RF results from Ross and Sheaffer (2014), who found that solid-fueled rockets have the second largest positive RF after RP1-fueled rockets. We likely underestimate the warming impact from solid-fueled rockets by not including the radiative effects of alumina particles, which Ross and Sheaffer (2014) estimated to account for up to 28% of the total RF from spaceflight. Maloney et al. (2025) found a TOA RF ranging between -9.62 mW/m^2 and 1.87 mW/m^2 for 10 Gg/yr of reentry Al_2O_3 emissions, where the variation depends on re-entry latitude and aerosol distribution. Alumina can have a positive or negative radiative effect, depending on their optical properties, altitude and particle size distribution, but these are currently poorly understood (Ferreira et al., 2024; Maloney et al., 2025; Ross & Sheaffer, 2014; Ryan et al., 2022; Danilin, Ko, & Weisenstein, 2001).

3.4. Limitations

In this work we develop a bottom-up spaceflight emission inventory for 2022 and investigate its atmospheric impacts. In doing so, we only account for launches and re-entry objects that could be geolocated. By not accounting for the emissions of re-entries that we could not locate, we underestimate the re-entry mass and subsequent emissions by 17%. We also do not account for Al_2O_3 particles formed from re-entry and their subsequent interactions with radiative forcing and chemistry, nor do we include emissions that are created by the burning of propellant during controlled re-entry. It is therefore likely that we also underestimate stratospheric ozone depletion and radiative effects from re-entry emissions. The chemistry transport model we use also does not account for self-lofting effects that may extend the lifetime of BC emissions (Yu et al., 2019), which may lead to larger effects on RF from BC as well as larger effects on ozone through increased surface areas for heterogeneous chemistry. We note that our estimations for the NO_x emissions generated by re-entry are based on simple approximations and come with substantial uncertainty. We also note that we consider a higher fraction of NO_x emissions from re-entry components compared to the work by Barker et al. (2024), which likely results in an overestimation of the ozone depletion effects of re-entry emissions. Despite this, we identify that re-entry emissions are an important factor in the atmospheric and climate effect of spaceflight, and we warrant that further research is needed to refine estimates of re-entry emissions.

The modeling of plume reactions is based on limited data from earlier works. Plume measurements have only been done for rockets that are no longer in use such as the Titan IV and Delta II (Ross et al., 1997, 2000), and

detailed simulations have mostly focussed on the Space Shuttle (Leone & Turns, 1994; Zittel, 1994). The absence of data for current active rockets introduces uncertainties in our model. Modern rocket engines tend to have higher combustion temperatures and a higher efficiency (Halchak et al., 2018) but do not necessarily have a hotter exhaust flow. Reusable engines, such as the Merlin engine of the Falcon 9, notably have a cooler exhaust flow than expendable engines (Wu & Zhang, 2023). To accurately assess the effects of plume reactions, in situ plume measurements for current rockets at multiple altitudes in the atmosphere are required.

Our results are specific to the fleet composition and emission scenario of 2022. The current development of liquid-methane-fueled rockets such as Starship, Vulcan Centaur and New Glenn will likely lead to different atmospheric and radiative effects. Liquid methane is assumed to have a smaller emission index for BC than RP1 (James et al., 2021; Wang et al., 2016), but measurements are needed to determine their exact emission products. For potential future scenarios of 450 and 2300 yearly launches we find an ozone decrease of 0.07% and 0.34% respectively. More detail on these future scenarios can be found in Text S4 of Supporting Information S1. Our study only considers the impact of emissions from rocket launches and re-entry. While it is estimated that the launch segment accounts for 99.87% of the observed ozone depletion (Wilson et al., 2022), detailed life-cycle analyses are needed to determine the full environmental impact of the space industry. For example, Maury et al. (2020) found that control centers and ground stations for space missions can account for roughly 25% of the total global warming potential of spaceflight due to their energy consumption.

4. Conclusions

Our study presents the atmospheric impacts of different aspects of spaceflight. We, for the first time, include the effects of chemical reactions in the rocket plume in setting up a global emission inventory, leading to emission indices that vary with altitude. We find 20.3 Gg of H_2O, 0.4 Gg of BC, 3.5 Gg of NO_x and 1.0 Gg of chlorine emissions for the year 2022. Re-entry of rocket bodies and satellites accounts for 83.9% of the NO_x emissions, while the inclusion of plume reactions decreases the total BC emissions by 66.8%.

We find that 2022 spaceflight emissions result in a global column ozone decrease of 85.6 mDU with a peak decrease in the Arctic region of 200 mDU. The largest ozone loss is caused by the NO_x- O_x loss cycle. We find a net TOA RF of 4.1 mW/m^2, with contributions from BC (8.2 mW/m^2), water vapor (-1.4 mW/m^2), ozone (-2.6 mW/m^2) and methane (-0.1 mW/m^2). Our emission-scaled BC RF of 20 mW/m^2 per Gg of propellant burned is higher than in previous studies due to a larger fraction of BC emissions occurring above the tropopause.

We find that re-entry emissions play a crucial role in ozone depletion, being responsible for 87.7% of the global column ozone depletion and driving the NO_x-O_x loss cycle. Despite their large impact on ozone loss, they only account for an ozone radiative forcing of -0.16 mW/m^2. Excluding plume reactions leads to a column ozone decrease of 12.5 mDU. Plume reactions have a considerable effect on the radiative forcing from spaceflight, as we find a RF of 11.8 mW/m^2 for BC and -1.5 mW/m^2 for ozone when they are not considered. These results indicate that both re-entry and plume reactions should be included in future assessments of the atmospheric impact of spaceflight.

When evaluating the impact of different propellant types on ozone column depletion, we find that solid propellant has the largest contribution per propellant unit mass with a reduction of 2.7 mDU/Gg yr^{-1}. In contrast, RP1 propellant and UDMH exhibit ozone increases of 0.1 mDU/Gg yr^{-1} and 40 μDU/Gg yr^{-1}, respectively. RP1-fueled rockets generate the highest net radiative forcing, calculated to be 0.8 mW/m^2/Gg yr^{-1} primarily due to the significant radiative forcing from black carbon (0.2 mW/m^2/Gg yr^{-1}). Unlike previous studies, we find UDMH-fueled rockets to have the second largest relative radiative forcing (29 μW/m^2/Gg yr^{-1}), while we find a negative RF from LH2 and solid-fueled rockets. The RF effects of the latter are underestimated by not modeling alumina particles, which can have a positive or negative radiative forcing depending on their properties.

Although the current atmospheric impact of spaceflight is small, this is expected to change as the sector continues to grow. High-altitude NO_x emissions from re-entry play an important role, and the ongoing development of satellite mega-constellations will lead to a large influx of re-entry mass. We note that our estimate of re-entry emissions contains uncertainties, and more accurate modeling methods are required to provide a better estimate. The overall climate impact of spaceflight can likely be reduced by using more LH2-fueled rockets instead of the RP1-fueled rockets that now dominate the market, however the low density and cryogenic storage

requirements make LH2 less suitable for lower stages. The current development of liquid-methane rockets will likely reduce the climate impact of spaceflight, as methane is expected to produce less black carbon per unit mass than RP1, but further research is needed to determine how the effect of liquid-methane compares to current propellant types. As the space industry continues to grow, a better understanding of the effects of re-entry emissions, rocket plume chemistry and aerosols such as those from alumina is required, alongside in situ measurements of emissions from new rocket engines and propellant types.

Conflict of Interest

The authors declare no conflicts of interest relevant to this study.

Availability Statement

The results of this work were obtained using the GEOS-Chem High Performance v14.3.1 model (The International GEOS-Chem User Community, 2024). The atmospheric model used meteorological data from the MERRA-2 reanalysis (Gelaro et al., 2017), anthropogenic emissions from CEDSv2 (O'Rourke et al., 2021), aviation emissions from openAVEM (Quadros et al., 2022), and a several specialized emission inventories (Giglio et al., 2013; Liang et al., 2010; Murray, 2016; L. T. Murray et al., 2012; Ordóñez et al., 2012; Ott et al., 2010; Philip et al., 2017; Tzompa-Sosa et al., 2017; Xiao et al., 2008). Re-entry object characteristics and launch information were obtained from the ESA DISCOS database (Torre et al., 2001). Population exposure calculations used the LandScan global population data set (Sims et al., 2023). The processing and visualization of the results was done using Python 3.12.0, with support of the MatplotLib (The Matplotlib Development Team, 2023), Pandas (The Pandas Development Team, 2024) and Xarray libraries (Hoyer et al., 2023). The data on which this article is based are available in Vliex et al. (2026).

Acknowledgments
This research was carried out on the Dutch National Supercomputer Snellius with the support of the SURF cooperative using Grant EINF-8214. For determining the re-entry objects in 2022, we used information from ESA DISCOS (Database and Information System Characterising Objects in Space), a single-source reference for launch information, object registration details, launch vehicle descriptions, as well as spacecraft information for all trackable, unclassified objects. We acknowledge ESA's efforts to maintain and operate this database with its APIs. LandScan global population data was obtained from Oak Ridge National Library (Sims et al., 2023), and the MERRA-2 data has been provided by the Global modelling and Assimilation Office at NASA Goddard Space Flight Center.

References

Ailor, W. H. (2019). Hazards of reentry disposal of satellites from large constellations. *Journal of Space Safety Engineering*, *6*(2), 113–121. https://doi.org/10.1016/j.jsse.2019.06.005

Ban-Weiss, G. A., Cao, L., Bala, G., & Caldeira, K. (2012). Dependence of climate forcing and response on the altitude of black carbon aerosols. *Climate Dynamics*, *38*(5), 897–911. https://doi.org/10.1007/s00382-011-1052-y

Barker, C. R., Marais, E. A., & McDowell, J. C. (2024). Global 3D rocket launch and re-entry air pollutant and CO2 emissions at the onset of the megaconstellation era. *Scientific Data*, *11*(1), 1079. https://doi.org/10.1038/s41597-024-03910-z

Bekkki, S., Beck, J., Lips, T., Merrifield, J., Spel, M., & Langener, T. (2021). *Environmental impacts of atmospheric emissions from spacecraft re-entry demise project: Atmospheric impact of spacecraft demise (atispade)*. European Space Agency. Retrieved from https://indico.esa.int/event/321/contributions/6403/attachments/4335/6538/esa-csid-21-bekki.pdf

Bennett, R. R., Hinshaw, J. C., & Barnes, M. W. (1992). The effects of chemical propulsion on the environment. *Acta Astronautica*, *26*(7), 531–541. https://doi.org/10.1016/0094-5765(92)90124-2

Blanchet, J.-P. (1985). On radiative heating due to polar stratospheric clouds. *Tellus B: Chemical and Physical Meteorology*, *37*(4–5), 197. https://doi.org/10.3402/tellusb.v37i4-5.15024

Boley, A. C., & Byers, M. (2021). Satellite mega-constellations create risks in Low Earth Orbit, the atmosphere and on Earth. *Scientific Reports*, *11*(1), 10642. https://doi.org/10.1038/s41598-021-89909-7

Brown, T. F., Bannister, M. T., & Revell, L. E. (2023). Envisioning a sustainable future for space launches: A review of current research and policy. *Journal of the Royal Society of New Zealand*, *54*(3), 273–289. https://doi.org/10.1080/03036758.2022.2152467

Brown, T. F., Bannister, M. T., Revell, L. E., Sukhodolov, T., & Rozanov, E. (2024). Worldwide rocket launch emissions 2019: An inventory for use in global models. *Earth and Space Science*, *11*(10), e2024EA003668. https://doi.org/10.1029/2024EA003668

Casalino, L., Ferrero, A., Masseni, F., & Pastrone, D. (2022). Emission-driven hybrid rocket engine optimization for small launchers. *Aerospace*, *9*(12), 807. https://doi.org/10.3390/aerospace9120807

Chávez, V. M., Añel, J. A., Garcia, R. R., Šácha, P., & Torre, L. D. L. (2022). Impact of increased vertical resolution in WACCM on the climatology of major sudden stratospheric warmings. *Atmosphere*, *13*(4), 546. https://doi.org/10.3390/atmos13040546

Checa-Garcia, R., Hegglin, M. I., Kinnison, D., Plummer, D. A., & Shine, K. P. (2018). Historical tropospheric and stratospheric ozone radiative forcing using the CMIP6 database. *Geophysical Research Letters*, *45*(7), 3264–3273. https://doi.org/10.1002/2017GL076770

Chiodo, G., & Polvani, L. M. (2022). New insights on the radiative impacts of ozone-depleting substances. *Geophysical Research Letters*, *49*(10), e2021GL096783. https://doi.org/10.1029/2021GL096783

Dallas, J. A., Raval, S., Alvarez Gaitan, J. P., Saydam, S., & Dempster, A. G. (2020). The environmental impact of emissions from space launches: A comprehensive review. *Journal of Cleaner Production*, *255*, 120209. https://doi.org/10.1016/j.jclepro.2020.120209

Danilin, M. Y., Ko, M. K., & Weisenstein, D. K. (2001a). Global implications of ozone loss in a space shuttle wake. *Journal of Geophysical Research*, *106*(D4), 3591–3601. https://doi.org/10.1029/2000JD900632

Danilin, M. Y., Shia, R.-L., Ko, M. K. W., Weisenstein, D. K., Sze, N. D., Lamb, J. J., et al. (2001b). Global stratospheric effects of the alumina emissions by solid-fueled rocket motors. *Journal of Geophysical Research*, *106*(D12), 12727–12738. https://doi.org/10.1029/2001JD900022

Denison, R. M., Lamb, J. J., Bjorndahl, W. D., Wong, E. Y., & Lohn, P. D. (1994). Solid rocket exhaust in the stratosphere - Plume diffusion and chemical reactions. *Journal of Spacecraft and Rockets*, *31*(3), 435–442. https://doi.org/10.2514/3.26457

DeSain, J., & Brady, B. (2014). Potential atmospheric impact generated by space launches worldwide—update for emission estimates from 1985 to 2013 (Tech. Rep.). Space and Missile Systems Center, U.S. Air Force Space Command. Retrieved from https://www.researchgate.net/publication/235802139_Potential_Atmospheric_Impact_Generated_by_Space_Launches_Worldwide_Update_for_Emission_Estimates_from_1985_to_2011

Eastham, S. D., Fritz, T., Sanz-Morère, I., Prashanth, P., Allroggen, F. G., Prinn, R., et al. (2022). Impacts of a near-future supersonic aircraft fleet on atmospheric composition and climate. *Environmental Sciences: Atmosphere*, *2*(3), 388–403. https://doi.org/10.1039/D1EA00081K

Eastham, S. D., Weisenstein, D. K., & Barrett, S. R. (2014). Development and evaluation of the unified tropospheric–stratospheric chemistry extension (UCX) for the global chemistry-transport model GEOS-Chem. *Atmospheric Environment*, *89*, 52–63. https://doi.org/10.1016/j.atmosenv.2014.02.001

ESA. (2025). Discosweb – Database and information system characterizing objects in space [Dataset]. Retrieved from https://discosweb.esoc.esa.int/objects

Fehlberg, E. (1970). Classical fourth- and lower order Runge-Kutta formulas with stepsize control and their application to heat transfer problems. NTRS Document ID: 19710043227 NTRS Research Center: Legacy CDMS (CDMS).

Ferreira, J. P., Huang, Z., Nomura, K.-I., & Wang, J. (2024). Potential ozone depletion from satellite demise during atmospheric reentry in the era of mega-constellations. *Geophysical Research Letters*, *51*(11), e2024GL109280. https://doi.org/10.1029/2024GL109280

Garner, R. J. (2022). *Modelling launch vehicle emissions in an evolving space sector*. University of Strathclyde. Retrieved from https://books.google.nl/books?id=JQxfzwEACAAJ

Gelaro, R., McCarty, W., Suárez, M. J., Todling, R., Molod, A., Takacs, L., et al. (2017). The modern-era retrospective analysis for research and applications, version 2 (MERRA-2) [Dataset]. *Journal of Climate*, *30*(14), 5419–5454. https://doi.org/10.1175/JCLI-D-16-0758.1

Giglio, L., Randerson, J. T., & van der Werf, G. R. (2013). Analysis of daily, monthly, and annual burned area using the fourth-generation global fire emissions database (GFED4) [Dataset]. *Journal of Geophysical Research: Biogeosciences*, *118*(1), 317–328. https://doi.org/10.1002/jgrg.20042

Gomberg, R. I., & Stewart, R. B. (1976). *A computer simulation of the afterburning process occurring within solid rocket motor plumes in the stratosphere* (Technical Report). National Aeronautics and Space Administration. Retrieved from https://ntrs.nasa.gov/api/citations/19770008588/downloads/19770008588.pdf

Grenfell, J. L., Lehmann, R., Mieth, P., Langematz, U., & Steil, B. (2006). Chemical reaction pathways affecting stratospheric and mesospheric ozone. *Journal of Geophysical Research*, *111*(D17). https://doi.org/10.1029/2004JD005713

Halchak, J. A., Cannon, J. L., & Brown, C. (2018). Materials for liquid propulsion systems. In *Aerospace materials and applications* (pp. 641–698). American Institute of Aeronautics and Astronautics, Inc. https://doi.org/10.2514/5.9781624104893.0641.0698

Heald, C. L., Ridley, D. A., Kroll, J. H., Barrett, S. R., Cady-Pereira, K. E., Alvarado, M. J., & Holmes, C. D. (2014). Contrasting the direct radiative effect and direct radiative forcing of aerosols. *Atmospheric Chemistry and Physics*, *14*(11), 5513–5527. https://doi.org/10.5194/acp-14-5513-2014

Hicke, J., & Tuck, A. (2001). Polar stratospheric cloud impacts on Antarctic stratospheric heating rates. *Quarterly Journal of the Royal Meteorological Society*, *127*(575), 1645–1658. https://doi.org/10.1002/qj.49712757510

Hodnebrog, y., Myhre, G., & Samset, B. H. (2014). How shorter black carbon lifetime alters its climate effect. *Nature Communications*, *5*(1), 5065. https://doi.org/10.1038/ncomms6065

Hoyer, S., Roos, M., Joseph, H., Magin, J., Cherian, D., Fitzgerald, C., et al. (2023). xarray [Software]. *Zenodo*. https://doi.org/10.5281/zenodo.8379187

Intergovernmental Panel on Climate Change (IPCC). (2001). Aerosols, their direct and indirect effects. In J. Houghton, Y. Ding, D. Griggs, M. Noguer, P. van der Linden, et al. (Eds.), *Climate change 2001: The scientific basis* (pp. 291–336). Cambridge University Press. https://doi.org/10.2307/20033020

Jackman, C., Considine, D., & Fleming, E. (1996). Space shuttle's impact on the stratosphere: An update. *Journal of Geophysical Research*, *101*(D7), 12523–12529. https://doi.org/10.1029/96JD00577

Jackman, C., Considine, D., & Fleming, E. (1998). A global modeling study of solid rocket aluminum oxide emission effects on stratospheric ozone. *Geophysical Research Letters*, *25*(6), 907–910. https://doi.org/10.1029/98GL00403

James, M. M., Lympany, S. V., Salton, A. R., Calton, M. F., Miake-Lye, R. C., & Wayson, R. L. (2021). *Commercial space vehicle emissions modeling* (Technical Report) (p. 26142). Transportation Research Board. https://doi.org/10.17226/26142

Kelley, M., Nicolls, M. J., Varney, R. H., Collins, R. L., Doe, R., Plane, J. M. C., et al. (2010). Radar, LiDAR, and optical observations in the polar summer mesosphere shortly after a space shuttle launch. *Journal of Geophysical Research*, *115*(A5). https://doi.org/10.1029/2009JA014938

Kim, Y., Lee, H., & Roh, T. (2021). Analysis of propellant weight under re-entry conditions for a reusable launch vehicle using retropropulsion. *Energies*, *14*(11), 3210. https://doi.org/10.3390/en14113210

Kokkinakis, I. W., & Drikakis, D. (2022). Atmospheric pollution from rockets. *Physics of Fluids*, *34*(5), 056107. https://doi.org/10.1063/5.0090017

Kravitz, B., Robock, A., Shindell, D. T., & Miller, M. A. (2012). Sensitivity of stratospheric geoengineering with black carbon to aerosol size and altitude of injection. *Journal of Geophysical Research*, *117*(D9). https://doi.org/10.1029/2011JD017341

Krebs, G. D. (2022). Orbital launches of 2022 [Dataset]. Retrieved from https://space.skyrocket.de/doc_chr/lau2022.htm

Lacis, A. A., Wuebbles, D. J., & Logan, J. A. (1990). Radiative forcing of climate by changes in the vertical distribution of ozone. *Journal of Geophysical Research*, *95*(D7), 9971–9981. https://doi.org/10.1029/JD095iD07p09971

Larson, E. J., Portmann, R. W., Rosenlof, K. H., Fahey, D. W., Daniel, J. S., & Ross, M. N. (2017). Global atmospheric response to emissions from a proposed reusable space launch system. *Earth's Future*, *5*(1), 37–48. https://doi.org/10.1002/2016EF000399

Lee, D. S., Fahey, D. W., Skowron, A., Allen, M. R., Burkhardt, U., Chen, Q., et al. (2021). The contribution of global aviation to anthropogenic climate forcing for 2000 to 2018. *Atmospheric Environment*, *244*, 117834. https://doi.org/10.1016/j.atmosenv.2020.117834

Leone, D., & Turns, S. (1994). Active chlorine and nitric oxide formation from chemical rocket plume afterburning. *32nd Aerospace Sciences Meeting and Exhibit*. https://doi.org/10.2514/6.1994-788

Liang, Q., Stolarski, R. S., Kawa, S. R., Nielsen, J. E., Douglass, A. R., Rodriguez, J. M., et al. (2010). Finding the missing stratospheric Br_y: A global modeling study of $CHBr_3$ and CH_2Br_2 [Dataset]. *Atmospheric Chemistry and Physics*, *10*(5), 2269–2286. https://doi.org/10.5194/acp-10-2269-2010

Lohn, P. D., Wong, E. P., Smith, T. W., Jr., Edwards, J. R., & Pilson, D. (1999). *Rocket exhaust impact on stratospheric ozone* (Technical Report). Defense Technical Information Center. https://doi.org/10.21236/ADA414282

Malkin, M. S. (1978). Environmental impact statement for the space shuttle program (Technical Report). Retrieved from https://ntrs.nasa.gov/api/citations/19810008106/downloads/19810008106.pdf

Maloney, C. M., Portmann, R. W., Ross, M. N., & Rosenlof, K. H. (2022). The climate and ozone impacts of black carbon emissions from global rocket launches. *Journal of Geophysical Research: Atmospheres*, *127*(12), e2021JD036373. https://doi.org/10.1029/2021JD036373

Maloney, C. M., Portmann, R. W., Ross, M. N., & Rosenlof, K. H. (2025). Investigating the potential atmospheric accumulation and radiative impact of the coming increase in satellite reentry frequency. *Journal of Geophysical Research: Atmospheres*, *130*(6), e2024JD042442. https://doi.org/10.1029/2024JD042442

Maury, T., Loubet, P., Serrano, S. M., Gallice, A., & Sonnemann, G. (2020). Application of environmental life cycle assessment (LCA) within the space sector: A state of the art. *Acta Astronautica*, *170*, 122–135. https://doi.org/10.1016/j.actaastro.2020.01.035

McBride, B. J., & Gordon, S. (1994). *Computer program for calculation of conmplex chemical equilibrium compositions and applications* (Vol. 1311). NASA Reference Publication. Retrieved from https://ntrs.nasa.gov/api/citations/19950013764/downloads/19950013764.pdf

McConnaughey, P. K., Femminineo, M. G., Koelfgen, S. J., Lepsch, R. A., Ryan, R. M., & Taylor, S. A. (2012). NASA's launch propulsion systems technology roadmap. Retrieved from https://ntrs.nasa.gov/citations/20120014957

Muelhaupt, T. J., Sorge, M. E., Morin, J., & Wilson, R. S. (2019). Space traffic management in the new space era. *Journal of Space Safety Engineering*, *6*(2), 80–87. https://doi.org/10.1016/j.jsse.2019.05.007

Murray (2016). Lightning NOxand impacts on air quality [Dataset]. *Current Pollution Reports*, *2*(2), 115–133. https://doi.org/10.1007/s40726-016-0031-7

Murray, L. T., Jacob, D. J., Logan, J. A., Hudman, R. C., & Koshak, W. J. (2012). Optimized regional and interannual variability of lightning in a global chemical transport model constrained by LIS/OTD satellite data [Dataset]. *Journal of Geophysical Research*, *117*(D20). https://doi.org/10.1029/2012JD017934

Ordóñez, C., Lamarque, J.-F., Tilmes, S., Kinnison, D. E., Atlas, E. L., Blake, D. R., et al. (2012). Bromine and iodine chemistry in a global chemistry-climate model: Description and evaluation of very short-lived oceanic sources [Dataset]. *Atmospheric Chemistry and Physics*, *12*(3), 1423–1447. https://doi.org/10.5194/acp-12-1423-2012

O'Rourke, P. R., Smith, S. J., Mott, A., Ahsan, H., McDuffie, E. E., Crippa, M., et al. (2021). CEDS v_2021_02_05 release emission data [Dataset]. *Zenodo*. https://doi.org/10.5281/zenodo.4509372

Ott, L. E., Pickering, K. E., Stenchikov, G. L., Allen, D. J., DeCaria, A. J., Ridley, B., et al. (2010). Production of lightning NO and its vertical distribution calculated from three-dimensional cloud-scale chemical transport model simulations [Dataset]. *Journal of Geophysical Research*, *115*(D4). https://doi.org/10.1029/2009JD011880

Pardini, C., & Anselmo, L. (2021). Evaluating the impact of space activities in low Earth orbit. *Acta Astronautica*, *184*, 11–22. https://doi.org/10.1016/j.actaastro.2021.03.030

Pardini, C., & Anselmo, L. (2022). Effects of the deployment and disposal of mega-constellations on human spaceflight operations in low LEO. *Journal of Space Safety Engineering*, *9*(2), 274–279. https://doi.org/10.1016/j.jsse.2022.03.001

Park, C., & Rakich, J. V. (1980). Equivalent-cone calculation of nitric oxide production rate during space shuttle re-entry. *Atmospheric Environment*, *14*(8), 971–972. https://doi.org/10.1016/0004-6981(80)90011-6

Park, P. H., Navarro Laboulais, J., Leyland, P., & Mischler, S. (2021). Re-entry survival analysis and ground risk assessment of space debris considering by-products generation. *Acta Astronautica*, *179*, 604–618. https://doi.org/10.1016/j.actaastro.2020.09.034

Philip, S., Martin, R. V., Snider, G., Weagle, C. L., van Donkelaar, A., Brauer, M., et al. (2017). Anthropogenic fugitive, combustion and industrial dust is a significant, underrepresented fine particulate matter source in global atmospheric models [Dataset]. *Environmental Research Letters*, *12*(4), 044018. https://doi.org/10.1088/1748-9326/aa65a4

Pollack, J. B., & McKay, C. P. (1985). The impact of polar stratospheric clouds on the heating rates of the winter polar stratosphere. *Journal of the Atmospheric Sciences*. https://doi.org/10.1175/1520-0469(1985)042⟨0245:TIOPSC⟩2.0.CO;2

Pradon, C. V., Eastham, S. D., Chossière, G., Sabnis, J., Speth, R. L., Barrett, S. R. H., & André Jooste, J. (2023). Global three-dimensional emission inventory for launch vehicles from 2009 to 2018. *Journal of Spacecraft and Rockets*, *60*(3), 716–727. https://doi.org/10.2514/1.A35385

Quadros, F. D. A., Snellen, M., Sun, J., & Dedoussi, I. C. (2022). Global civil aviation emissions estimates for 2017–2020 using ADS-B data [Dataset]. *Journal of Aircraft*, *59*(6), 1394–1405. https://doi.org/10.2514/1.C036763

Ramaswamy, V., Collins, W., Haywood, J., Lean, J., Mahowald, N., Myhre, G., et al. (2018). Radiative forcing of climate: The historical evolution of the radiative forcing concept, the forcing agents and their quantification, and applications. *Meteorological Monographs*, *59*, 14.1–14.101. https://doi.org/10.1175/AMSMONOGRAPHS-D-19-0001.1

Revell, L., Bannister, M., Brown, T., Sukhodolov, T., Vattioni, S., Dykema, J., et al. (2025). Near-future rocket launches could slow ozone recovery. *npj Climate and Atmospheric Science*, *8*. https://doi.org/10.21203/rs.3.rs-5837547/v1

Ross, D., Weisenstein, D., & Ko, M. (2004). Ozone depletion caused by NO and H2O emissions from hydrazine-fueled rockets. *Journal of Geophysical Research D: Atmosphere*, *109*(21), D213051-7. https://doi.org/10.1029/2003JD004370

Ross, M., Mills, M., & Toohey, D. (2010). Potential climate impact of black carbon emitted by rockets. *Geophysical Research Letters*, *37*(24). https://doi.org/10.1029/2010GL044548

Ross, M., Toohey, D., Peinemann, M., & Ross, P. (2009). Limits on the space launch market related to stratospheric ozone depletion. *Astropolitics*, *7*(1), 50–82. https://doi.org/10.1080/14777620902768867

Ross, M. N., & Jones, K. L. (2022). Implications of a growing spaceflight industry: Climate change. *Journal of Space Safety Engineering*, *9*(3), 469–477. https://doi.org/10.1016/j.jsse.2022.04.004

Ross, M. N., & Sheaffer, P. M. (2014). Radiative forcing caused by rocket engine emissions. *Earth's Future*, *2*(4), 177–196. https://doi.org/10.1002/2013EF000160

Ross, T., Rawlins, W. T., Richard, E. C., Kelly, K. K., Tuck, A. F., Sheldon, W. R., et al. (2000). Observation of stratospheric ozone depletion associated with delta ii rocket emissions. *Geophysical Research Letters*, *27*(15), 2209–2212. https://doi.org/10.1029/1999GL011159

Ross, M. N., Ballenthin, J. O., Gosselin, R. B., Meads, R. F., Zittel, P. F., Benbrook, J. R., & Sheldon, W. R. (1997). In-situ measurement of Cl_2 and O_3 in a stratospheric solid rocket motor exhaust plume. *Geophysical Research Letters*, *24*(14), 1755–1758. https://doi.org/10.1029/97GL01592

Ross, M. N., & Toohey, D. W. (2019). The coming surge of rocket emissions. *Eos*, *100*. https://doi.org/10.1029/2019EO133493

Ross, M., & Vedda, J. A. (2018). *The policy and science of rocket emissions* (Technical Report). The Aerospace Conferation. Retrieved from https://aerospace.org/sites/default/files/2018-05/RocketEmissions_0.pdf

Ryan, R. G., Marais, E. A., Balhatchet, C. J., & Eastham, S. D. (2022). Impact of rocket launch and space debris air pollutant emissions on stratospheric ozone and global climate. *Earth's Future*, *10*(6), e2021EF002612. https://doi.org/10.1029/2021EF002612

Salawitch, R. J., Fahey, D. W., Hegglin, M. I., & McBride, L. A. (2019). *Scientific assessment of ozone depletion 2018: Twenty questions and answers about the ozone layer* (2018th ed.). World Meteorological Organization. Retrieved from https://csl.noaa.gov/assessments/ozone/2018/twentyquestions/

Schmid, O., Reeves, J. M., Wilson, J. C., Wiedinmyer, C., Brock, C. A., Toohey, D. W., et al. (2003). Size-resolved particle emission indices in the stratospheric plume of an Athena II rocket. *Journal of Geophysical Research*, *108*(D8). https://doi.org/10.1029/2002JD002486

Shutler, J., Yan, X., Cnossen, I., Schulz, A. L., Glaßmeier, K., Hawkins, N., & Nasu, H. (2022). Atmospheric impacts of the space industry require oversight. *Nature Geoscience*, *15*(8), 598–600. https://doi.org/10.1038/s41561-022-01001-5

Sims, K., Reith, A., Bright, E., Kaufman, J., Pyle, J., Epting, J., et al. (2023). LandScan Global 2022 [Dataset]. *Oak Ridge National Laboratory*. https://doi.org/10.48690/1529167

Solomon, S., Mills, M., Heidt, L. E., Pollock, W. H., & Tuck, A. F. (1992). On the evaluation of ozone depletion potentials. *Journal of Geophysical Research*, *97*(D1), 825–842. https://doi.org/10.1029/91JD02613

Stanevich, I., Jones, D. B. A., Strong, K., Parker, R. J., Boesch, H., Wunch, D., et al. (2020). Characterizing model errors in chemical transport modeling of methane: Impact of model resolution in versions v9-02 of GEOS-Chem and v35j of its adjoint model. *Geoscientific Model Development*, *13*(9), 3839–3862. https://doi.org/10.5194/gmd-13-3839-2020

Strahan, S. E., & Polansky, B. C. (2006). Meteorological implementation issues in chemistry and transport models. *Atmospheric Chemistry and Physics*, *6*(10), 2895–2910. https://doi.org/10.5194/acp-6-2895-2006

The International GEOS-Chem User Community. (2024). geoschem/GCHP: GCHP 14.3.1 [Software]. *Zenodo*. https://doi.org/10.5281/zenodo.10909030

The Matplotlib Development Team. (2023). Matplotlib: Visualization with Python [Software]. *Zenodo*. https://doi.org/10.5281/zenodo.8347255

The Pandas Development Team. (2024). pandas-dev/pandas: Pandas [Software]. *Zenodo*. https://doi.org/10.5281/zenodo.13819579

Torre, C., Pina Caballero, F., Sánchez-Ortiz, N., Sdunnus, H., & Klinkrad, H. (2001). Discos database and web interface. Retrieved from https://www.researchgate.net/publication/252802440_DISCOS_database_and_Web_interface

Trenberth, K., & Smith, L. (2005). The mass of the atmosphere: A constraint on global analyses. *Journal of Climate*, *18*(6), 864–875. https://doi.org/10.1175/JCLI-3299.1

Tritscher, I., Pitts, M. C., Poole, L. R., Alexander, S. P., Cairo, F., Chipperfield, M. P., et al. (2021). Polar stratospheric clouds: Satellite observations, processes, and role in ozone depletion. *Reviews of Geophysics*, *59*(2), e2020RG000702. https://doi.org/10.1029/2020RG000702

Tzompa-Sosa, Z. A., Mahieu, E., Franco, B., Keller, C. A., Turner, A. J., Helmig, D., et al. (2017). Revisiting global fossil fuel and biofuel emissions of ethane [Dataset]. *Journal of Geophysical Research: Atmospheres*, *122*(4), 2493–2512. https://doi.org/10.1002/2016JD025767

van Caspel, W., Simpson, D., Jonson, J. E., Benedictow, A. M. K., Ge, Y., di Sarra, A., et al. (2023). Implementation and evaluation of updated photolysis rates in the EMEP MSC-W chemistry-transport model using Cloud-*J* v7.3e. *Geoscientific Model Development*, *16*(24), 7433–7459. https://doi.org/10.5194/gmd-16-7433-2023

van't Hoff, J. A., Grewe, V., & Dedoussi, I. C. (2024). Sensitivities of ozone and radiative forcing to supersonic aircraft emissions across two flight corridors. *Journal of Geophysical Research: Atmospheres*, *129*(22), e2023JD040476. https://doi.org/10.1029/2023JD040476

van't Hoff, J. A., Hauglustaine, D., Pletzer, J., Skowron, A., Grewe, V., Matthes, S., & Dedoussi, I. C. (2025). Multi-model assessment of the atmospheric and radiative effects of supersonic transport aircraft. *Atmospheric Chemistry and Physics*, *25*(4). https://doi.org/10.5194/acp-25-2515-2025

Vliex, Y., van't Hoff, J., & Dedoussi, I. C. (2026). Supporting dataset for "The role of propellant type, re-entry, and plume reactions in the atmospheric impacts of spaceflight" (Version 1) [Dataset]. *4TU.ResearchData*. https://doi.org/10.4121/00e10811-8513-453f-bcae-63e394439200.v1

Voigt, C., Schumann, U., Graf, K., & Gottschaldt, K. D. (2013). Impact of rocket exhaust plumes on atmospheric composition and climate—An overview. *Progress in Propulsion Physics*, *4*, 657–670. https://doi.org/10.1051/eucass/201304657

Wang, Y., Xing, Z., Xu, H., & Du, K. (2016). Emission factors of air pollutants from CNG-gasoline bi-fuel vehicles: Part I. Black carbon. *Science of the Total Environment*, *572*, 1161–1165. https://doi.org/10.1016/j.scitotenv.2016.08.027

Wilson, A. R., Vasile, M., Maddock, C. A., & Baker, K. J. (2022). Ecospheric life cycle impacts of annual global space activities. *Science of the Total Environment*, *834*, 155305. https://doi.org/10.1016/j.scitotenv.2022.155305

Wu, H., & Zhang, Z. (2023). Analysis of the development of reusable launch vehicle technology. *Applied and Computational Engineering*, *11*(1), 65–75. https://doi.org/10.54254/2755-2721/11/20230209

Xiao, Y., Logan, J. A., Jacob, D. J., Hudman, R. C., Yantosca, R., & Blake, D. R. (2008). Global budget of ethane and regional constraints on U.S. sources [Dataset]. *Journal of Geophysical Research*, *113*(D21). https://doi.org/10.1029/2007JD009415

Yu, P., Toon, O. B., Bardeen, C. G., Zhu, Y., Rosenlof, K. H., Portmann, R. W., et al. (2019). Black carbon lofts wildfire smoke high into the stratosphere to form a persistent plume. *Science*, *365*(6453), 587–590. https://doi.org/10.1126/science.aax1748

Zhang, J., Wuebbles, D., Kinnison, D., & Baughcum, S. L. (2021a). Potential impacts of supersonic aircraft emissions on ozone and resulting forcing on climate: An update on historical analysis. *Journal of Geophysical Research: Atmospheres*, *126*(6), e2020JD034130. https://doi.org/10.1029/2020JD034130

Zhang, J., Wuebbles, D., Kinnison, D., & Baughcum, S. L. (2021b). Stratospheric ozone and climate forcing sensitivity to cruise altitudes for fleets of potential supersonic transport aircraft. *Journal of Geophysical Research: Atmospheres*, *126*(16), e2021JD034971. https://doi.org/10.1029/2021JD034971

Zhang, J., Wuebbles, D., Pfaender, J., Kinnison, D., & Davis, N. (2023). Potential impacts on ozone and climate from a proposed fleet of supersonic aircraft. *Earth's Future*, *11*(4), e2022EF003409. https://doi.org/10.1029/2022EF003409

Zittel, P. (1994). Computer model predictions of the local effects of large, solid-fuel rocket motors on stratospheric ozone (Technical Report). Retrieved from https://apps.dtic.mil/sti/pdfs/ADA285632.pdf

References From the Supporting Information

Alexeenko, A. A., Gimelshein, N. E., Levin, D. A., Collins, R. J., Rao, R., Candler, G. V., et al. (2002). Modeling of flow and radiation in the ATLAS plume. *Journal of Thermophysics and Heat Transfer*, *16*(1), 50–57. https://doi.org/10.2514/2.6651

Ben, M., & Yohai, V. (2004). Quantile–Quantile plot for deviance residuals in the generalized linear model. *Journal of Computational & Graphical Statistics*, *13*(1), 36–47. https://doi.org/10.1198/1061860042949

Calabuig, G. J., Miraux, L., Wilson, A., Pasini, A., & Sarritzu, A. (2022). Eco-design of future reusable launchers: Insight into their life cycle and atmospheric impact. In *Proceedings of the 9th European conference for aeronautics and space sciences*. https://doi.org/10.13009/EUCASS2022-7353

Falle, A., Wright, E., Boley, A., & Byers, M. (2023). One million (paper) satellites. *Science*, *382*(6667), 150–152. https://doi.org/10.1126/science.adi4639

Gauss, M., Isaksen, I. S. A., Wong, S., & Wang, W. C. (2003). Impact of H_2O emissions from cryoplanes and kerosene aircraft on the atmosphere. *Journal of Geophysical Research*, *108*(D10), 4304. https://doi.org/10.1029/2002JD002623

Jordan, C. E., Dibb, J. E., & Finkel, R. C. (2003). 10Be/^{7}Be tracer of atmospheric transport and stratosphere–troposphere exchange. *Journal of Geophysical Research*, *108*(D8), 4234. https://doi.org/10.1029/2002JD002395

Karagodin-Doyennel, A., Rozanov, E., Kuchar, A., Ball, W., Arsenovic, P., Remsberg, E., et al. (2021). The response of mesospheric H_2O and CO to solar irradiance variability in models and observations. *Atmospheric Chemistry and Physics*, *21*(1), 201–216. https://doi.org/10.5194/acp-21-201-2021

Koo, J., Wang, Q., Henze, D. K., Waitz, I. A., & Barrett, S. R. H. (2013). Spatial sensitivities of human health risk to intercontinental and high-altitude pollution. *Atmospheric Environment*, *71*, 140–147. https://doi.org/10.1016/.atmosenv.2013.01.025

Lee, D. S., Fahey, D. W., Forster, P. M., Newton, P. J., Wit, R. C. N., Lim, L. L., & Sausen, R. (2009). Aviation and global climate change in the 21st century. *Atmospheric Environment*, *43*(22), 3520–3537. https://doi.org/10.1016/j.atmosenv.2009.04.024

Magee, J., Bruno, T. J., Friend, D. G., Huber, M. L., Laesecke, A., Lemmon, E. W., et al. (2009). Thermophysical properties measurements and models for rocket propellant RP-1: Phase I. *Journal of Propulsion and Power*, *25*(5), 1009–1025. https://doi.org/10.2514/1.40543

Myhre, G., Shindell, D., Bréon, F.-M., Collins, W., Fuglestvedt, J., Huang, J., & Zhang, H. (2013). Anthropogenic and natural radiative forcing. In T. F. Stocker, et al. (Eds.), *Climate change 2013: The physical science basis. Contribution of working group I to the fifth assessment report of the intergovernmental panel on climate change* (pp. 659–740). Cambridge University Press.

Nascimento, E. G., Souza, N. B. P., Kitagawa, Y. K. L., & Moreira, D. M. (2018). Simulated dispersion of the gas released by the SpaceX Falcon 9 rocket explosion. *Journal of Spacecraft and Rockets*, *55*(6), 1528–1536. https://doi.org/10.2514/1.A34145

Nascimento, E. G. S., Souza, N. B. P. D., & Moreira, D. M. (2019). Evaluating the impact of HCl atmospheric dispersion caused by an aborted rocket launch under different stability conditions. *International Journal of Advanced Engineering Research and Science*, *6*(7), 577–585. https://doi.org/10.22161/ijaers.6764

Ningombam, S., Vemareddy, P., & Song, H. J. (2018). The recent signs of total column ozone recovery over mid-latitudes: The effects of the Montreal Protocol mandate. *Journal of Atmospheric and Solar-Terrestrial Physics*, *178*, 32–46. https://doi.org/10.1016/j.jastp.2018.05.011

Poole, M. A., & O'Farrell, P. N. (1971). The assumptions of the linear regression model. *Transactions of the Institute of British Geographers*, *52*, 145–158. https://doi.org/10.2307/621706

Quadros, F. D., Snellen, M., & Dedoussi, I. C. (2020). Regional sensitivities of air quality and human health impacts to aviation emissions. *Environmental Research Letters*, *15*(10), 105013. https://doi.org/10.1088/1748-9326/abb2c5

Shahar, S. (n.d.). Telemetry-Data [Software]. *GitHub*. https://github.com/shahar603/Telemetry-Data

Shapiro, S. S., & Wilk, M. B. (1965). An analysis of variance test for normality (complete samples). *Biometrika*, *52*(3–4), 591–611. https://doi.org/10.2307/2333709

Shu, J., Kim, J., Lee, J., & Kim, S. (2015). Multidisciplinary mission design optimization for space launch vehicles based on sequential design process. *Proceedings of the Institution of Mechanical Engineers, Part G: Journal of Aerospace Engineering*, *230*(1), 3–18. https://doi.org/10.1177/0954410015586858

Waswa, P., & Hoffman, J. (2012). Illustrative NASA low Earth orbit spacecraft subsystems design-for-demise trade-offs, analyses and limitations. *International Journal of Design Engineering*, *5*(1), 21–40. https://doi.org/10.1504/IJDE.2012.050280

Weber, M., Coldewey-Egbers, M., Fioletov, V. E., Frith, S. M., Wild, J. D., Burrows, J. P., & Loyola, D. (2018). Total ozone trends from 1979 to 2016 derived from five merged observational datasets: The emergence into ozone recovery. *Atmospheric Chemistry and Physics*, *18*(3), 2097–2117. https://doi.org/10.5194/acp-18-2097-2018

Wilcox, L. J., Shine, K. P., & Hoskins, B. J. (2012). Radiative forcing due to aviation water vapour emissions. *Atmospheric Environment*, *63*, 1–13. https://doi.org/10.1016/j.atmosenv.2012.08.072

Yap, B. W., & Sim, C. H. (2011). Comparisons of various types of normality tests. *Journal of Statistical Computation and Simulation*, *81*(12), 2141–2155. https://doi.org/10.1080/00949655.2010.520163